Structure of the Drosophila ALKA chloride channel responsible for alkaline taste sensation

Jiaxian Xiao[1#], Yu Jia[2#], Mingyu Gong[4], Yuqi Li[4], Weiping Li[4], Dandan Qian[4*], Huahua Sun[3*], Renhong Yan[2*], Deshun Gong[4*]

[1]State Key Laboratory of Medicinal Chemical Biology and College of Chemistry,
Nankai University, Tianjin 300350, China.

[2] Department of Biochemistry, SUSTech Homeostatic Medicine Institute, Key
University Laboratory of Metabolism and Health of Guangdong, School of Medicine,
Institute for Biological Electron Microscopy, Southern University of Science and
Technology, Shenzhen 518055, Guangdong, China.

[3]State Key Laboratory and Institute of Elemento-Organic Chemistry, National Engineering Research Center of Pesticide, College of Chemistry, Nankai University, Tianjin 300071, China.

[4]State Key Laboratory of Medicinal Chemical Biology and College of Life Sciences, Nankai University, Tianjin 300350, China.

[#]These authors contributed equally to this work.

[*]To whom correspondence should be addressed:

qiandd@nankai.edu.cn; sunhuahua@nankai.edu.cn;

yanrh@sustech.edu.cn; gongds@nankai.edu.cn.

Abstract

The ALKA channel, a member of the Cys-loop ligand-gated ion channel (cysLGIC) family, has recently been identified as a receptor mediating alkaline taste sensation in Drosophila. However, the structure and molecular mechanism underlying pH sensing of ALKA channel remain to be determined. Here, we report the cryo-EM structure of ALKA, determined at a resolution of 2.86 Å under its physiological pH condition. ALKA forms a symmetric pentamer featuring a V-shaped pore architecture with a progressive constriction-to-expansion profile extending from its intracellular base toward the extracellular side. The primary constriction site is composed of five P276 residues, forming a narrow gate with a pore radius of approximately 1.6 Å-consistent with a closed state. The secondary constriction site, formed by five T280 residues (T280 ring), exhibits a similar pore radius of approximately 1.7 Å. At this site, a putative chloride ion is anchored through cooperative interactions involving both the T280 and T284 rings. Structural mapping reveals that five lysine residues as strong candidates for functional pH sensing, with K229 most likely serving as the principal sensor owing to its strategic position in loop C. This structure serves as an

important basis for understanding the functional mechanisms of the ALKA channel.

Introduction

Cys-loop ligand-gated ion channels (cysLGICs) constitute a superfamily best known for mediating neurotransmitter actions in signal transmission throughout the nervous system. Mammalian cysLGICs typically include the nicotinic acetylcholine receptor (nAChR), serotonin receptor (5-HT_3R), glycine receptor (GlyR), gamma-aminobutyric acid A receptor ($GABA_A$R), and a recently identified zinc-activated channel (ZAC)[1-3]. In contrast, insect cysLGICs include nAChRs and GABA receptors, but also feature glutamate-gated chloride channels (GluCls), pH-sensitive chloride channels (pHCls), and histamine-gated chloride channels (HACls)-receptors that are exclusively found in invertebrates[4]. Members of the cysLGIC superfamily mediate both fast excitatory and inhibitory synaptic transmission in vertebrates and invertebrates, making them important targets for therapeutic drugs and insecticides[5].

pHCls are invertebrate-specific members of cysLGICs and are particularly sensitive to pH changes that occur during metabolic shifts or stress responses[6-10]. Acids and bases are opposing chemical substances that are prevalent in food[11]; accordingly, the sense of taste serves as an initial protective barrier prior to ingestion in insects and thus requires the ability to evaluate environmental pH[12]. Although mechanisms that mediate sour taste

and acid sensing have been reported across species[13-15], relatively little is known about the detection of high pH or basic substances. In 2023, Yali Zhang's group identified a chloride ion channel named ALKA that is directly activated by hydroxide ions (OH^-) or high pH and is responsible for alkaline taste perception in Drosophila[10]. ALKA is a member of cysLGICs and shows a low level of homology (~30% identity) to vertebrate GlyRs[10]. Although ALKA was proposed to be a sensor for OH^- in their study, it remains to be determined whether ALKA-mediated alkaline taste sensing occurs through OH^- acting as a specific ligand or through the deprotonation of certain side chains (such as lysine) to disrupt interactions leading to channel opening in strongly alkaline environments.

Here, we report the cryo-electron microscopy (cryo-EM) structure of ALKA at 2.86 Å resolution under pH 7.4 conditions, which reveals that ALKA assembles into a homopentamer, consistent with the cysLGICs family. Although ALKA protein samples exhibit favorable behavior in gel filtration at pH 10-12, cryo-EM analysis reveals that prolonged exposure to high pH conditions leads to protein denaturation, preventing the determination of the open-state structure of ALKA under these conditions. Despite this

limitation, the structure of ALKA at pH 7.4 provides important insights into the channel.

Results

Structural determination of Drosophila ALKA channel

Since the Drosophila ALKA channel specifically responds to high pH conditions (pH 10–13)[10], we aimed to determine its structure under four distinct pH conditions to elucidate the dynamic conformational changes associated with alkaline taste sensation. Condition 1 was set to pH 7.4 and used to mimic the physiological pH environment of gustatory receptor neurons in fruit flies; Conditions 2-4 were set to pH 10-12, respectively, and used to mimic high-pH stimuli in a gradient manner (Supplementary Fig. S1). The 2D class averages clearly indicated that the ALKA channel loses its structural features under Conditions 2-4, in contrast to the distinct features of the transmembrane and extracellular regions, as well as the symmetrical characteristics of the ALKA channel under Condition 1 (Supplementary Fig. S1). These results suggest that the structure of the ALKA channel is disrupted following prolonged exposure to high-pH conditions. Accordingly, we were only able to obtain the structure of the ALKA channel at pH 7.4.

The detailed protocols for protein purification, sample preparation, cryo-EM data acquisition, and structural determination are described in the Materials and Methods section, accompanied by Supplementary Figs. S1-S5 and Table S1. The structure of ALKA in Condition 1 was determined at an overall resolution of 2.86 Å, exhibiting excellent main chain connectivity and side chain densities in the extracellular and transmembrane domains (ECD and TMD). Similar to other members of the cysLGIC family, the long intracellular domain (ICD) between transmembrane helix 3 (M3) and helix 4 (M4) was almost invisible in the map, reflecting its intrinsic flexibility.

Structure of ALKA

The Drosophila ALKA gene encodes a 449-amino acid (aa) protein and a 445-aa isoform. As observed in all members of the cysLGIC family with available structures, the 445-aa ALKA isoform in this study also forms a pentameric structure. Viewed perpendicular to the central five-fold symmetry axis, the ALKA channel approximates a cylinder 115 Å in height, with a diameter ranging from 65 to 88 Å (Fig. 1a, b). Viewed along the same symmetry axis from the extracellular side, the pentamer exhibits a pentagonal profile with a side length of approximately 49 Å, surrounded by ten N-linked

glycans (two per subunit) (Fig. 1b).

Similar to all cysLGIC family subunits, ALKA exhibits a conserved transmembrane topology and consists of three distinct structural domains: the extracellular domain (ECD), the transmembrane domain (TMD), and the intracellular domain (ICD). The ECD is composed of ten β-strands organized into an inner β-sheet, comprising β-strands 1, 2, 3, 5, 6, and 8, and an outer β-sheet, comprising β-strands 4, 7, 9, and 10 (Fig. 2a). A series of structural elements involved in ligand binding and coupling to channel gating within the ECD of the cysLGIC family have been well characterized[16-18]. These include the ligand-binding pocket formed by six loops referred to as loop A-F, and an allosteric network located at the interface between the ECD and the TMD that couples the binding pocket to the gating machinery, comprising loop 2, the Cys-loop, loop F, and the M2-M3 loop within the TMD (Fig. 2b)[19]. Due to the highly conserved topology of ALKA with other members of the cysLGIC family, the corresponding regions can be reliably mapped onto the ALKA structure (Fig. 2a, b).

Among them, loop C has been proposed to act as the mechanical link that couples extracellular ligand binding to transmembrane

pore gating, owing to its substantial conformational rearrangement upon agonist binding and channel activation-a process referred to as capping or contraction, wherein “capping” refers to its displacement toward the long axis of the channel during the transition from the unliganded closed state to the agonist-bound open or desensitized state[18]. In contrast, the turn of ALKA loop C is inserted into the binding pocket and locked by interactions among K229-a unique interaction residue observed in ALKA-and E182 as well as Y124 (Fig. 2c, d), resulting in steric hindrance upon ligand binding (Fig. 2d and Supplementary Fig. S6c-f), as reflected by the lack of response from ALKA upon stimulation with glycine and GABA in electrophysiological studies[10]. As the pKa values of the phenolic hydroxyl group in tyrosine and the ε-amino group of lysine are approximately pH 10, close to the pH threshold for ALKA channel activation, deprotonation occurs under highly alkaline conditions (pH 11-13). Consequently, the ionic interactions between K229 and E182, as well as the cation-π interactions and hydrogen bond between K226 and Y124, may be weakened or disrupted, thereby increasing the flexibility of loop C and potentially affecting channel gating during alkaline taste sensation.

The TMD is comprised of four transmembrane helices (M1-M4),

wherein the M2 helix from the five protomers forms the ion-conducting pore. The ICD is resolved as only two β-strands, reflecting its intrinsic flexibility (Fig. 2a).

Ion-conducting pathway

The ALKA channel possesses a central chloride-conducting pathway located along its five-fold symmetric axis, forming a V-shaped pore with a bottom-up constriction-to-expansion profile (Fig. 3a). This feature resembles the structure of the desensitized state of its closest structural homolog GlyR[20] (Supplementary Fig. S6a, b), even though our structure was determined at physiological pH, a closed state theoretically. This observation indicates that ALKA may have a distinct closed-open-desensitization mechanism, the principal gating cycle conformations adopted by the cysLGIC family[21].

Five proline residues (P276), located on the cytoplasmic side of the M2 helix within the pentameric assembly, form the constriction site with a pore radius of approximately 1.6 Å (Fig. 3a), consistent with a closed state, as the chloride ion has a radius of approximately 1.8 Å. In addition, three threonine rings (T280, T284 and T291) are positioned immediately above the constriction site when viewed

from the extracellular side, with the T280 ring forming the second constriction site with a pore radius of approximately 1.7 Å (Fig. 3a). Notably, an additional density that may correspond to a chloride ion is observed between the T280 and T284 rings, located closer to the T280 ring (Fig. 3b). Due to the proximity of the T280 ring to the P276 constriction site, the T280 and T284 rings may transiently accommodate chloride ions, serving as a substitute for the hydration shell of the chloride ion and thereby stabilizing its transition state during passage through the channel[16,22]. A chloride ion coordinated by a threonine ring has also been observed in the structures of GluCl[16] channel (Supplementary Fig. S7b). In addition, the channel blocker picrotoxin is also coordinated by a threonine ring in the structure of GlyR[23] (Supplementary Fig. S7a). These observations indicate that the T280 ring, flanking the proline gating residue of ALKA, has a potentially important role in ion selectivity and channel gating.

Structural mapping of lysine residues predicts the potential pH sensing residues

Given that the ALKA channel activates at approximately pH 10-coinciding closely with the p*K*a of the lysine ε-amino group-the involvement of lysine residues in pH-dependent gating is strongly

implicated. To identify lysine residues potentially involved in pH sensing, the following criteria were applied: (i) solvent accessibility; (ii) likely functional uniqueness-reflected by an unusually alkaline half-maximal activation pH (pH_{50} = 11.9)[10], which differentiates ALKA from other characterized pHCls; (iii) structural capacity to engage in a key ionic interaction whose stability is modulated by protonation of the ε-amino group; and (iv) likely localization within conserved structural elements essential for channel activation in the cysLGIC family. Of the 12 lysine residues in the ECD of ALKA, 11 were reliably mapped to the structural model (Fig. 4a); among these, 8 participate in ionic interactions, whereas K53, K54, and K139 do not (Fig. 4b). Sequence alignment of ALKA with other cysLGIC family members-including GlyRs, pHCls, and the RDL (resistance to dieldrin) receptor-reveals that lysine residues K149, K190, K192, K207, and K229 are specific to ALKA, but not K49, K129, and K147 (Supplementary Fig. S5).

K149, located in β6 (designated as loop E within the ligand-binding pocket of cysLGICs), forms an ionic interaction with E95 in loop β2-β3 (Fig. 4c). Similarly, K190, situated in loop B, engages in interprotomeric ionic interactions with E102’ and D105’ in the loop

β2-β3 of the adjacent protomer (Fig. 4d). K192, located in β8, forms intraprotomeric ionic interactions with E221 and D223 in β9, likely contributing to the structural stabilization of loop C (Fig. 4e). Notably, K229, located in loop C, locked the loop C in an inward conformation (Fig. 2d). Collectively, these four lysine residues all surround the ligand-binding pocket of the cysLGIC family; among them, K229 occupies the central position within the orthosteric site and is therefore the most functionally plausible pH sensor (Fig. 4g). Finally, K207, positioned in loop F, forms an interprotomeric ionic interaction with E166’ in the Cys-loop of the neighboring protomer (Fig. 4f), an interaction situated within the conserved transduction coupling region of the cysLGIC family. Collectively, these five lysine residues fulfill the structural and physicochemical criteria required for pH sensing and are thus strong candidates for functional pH sensors.

Discussion

The sense of taste plays a crucial role in shaping human food experiences by serving as an initial protective mechanism prior to ingestion. Likewise, animals must avoid ingesting foods with strongly acidic or alkaline pH levels to ensure survival. Recently, an increasing number of alkaline-sensing receptors have been

identified in invertebrates. In addition to the ALKA and pHCls in the cysLGIC superfamily, transmembrane channel-like 1 (TMC1) in nematodes-the ortholog of the human auditory mechanosensory receptor-has been shown to play an unexpected role in alkaline sensation via nociceptive neurons[24]. Furthermore, the transmembrane receptor-type guanylyl cyclase GCY-14 in the gustatory neurons of nematodes has been demonstrated to be essential for sensing extracellular alkalinity[25]. In Drosophila, ionotropic receptors are critically involved in high-pH perception[26]. However, the molecular mechanisms of alkali-sensing remain poorly understood.

In this study, the closed-state structure of the ALKA channel has been determined at 2.86 Å resolution, enabling elucidation of its structural details. Interestingly, a putative chloride ion was identified between the T280 and T284 rings (Fig. 3b), suggesting their potentially important roles in coordinating the ion as it moves through the channel. Owing to the lack of an activated ALKA structure under high-pH conditions, it remains unclear whether hydroxide ions act as specific activating ligands. Four lysine residues surrounding the ligand-binding pocket of the cysLGIC family, along with an additional lysine in the coupling region, are

predicted to participate in pH sensing. Among these, K229 likely serves as the primary pH sensor due to its key location within loop C. This suggests that ALKA channel gating may be regulated by a long-range allosteric mechanism, analogous to the gating triggered by orthosteric ligand binding across the cysLGIC superfamily. Our work marks an important step towards elucidating the molecular mechanisms of ALKA.

Materials and methods

Transient protein expression and purification

The full-length Drosophila *ALKA* cDNA (A0A0B4LF41_DROME) was subcloned into the pCAG vector with a His6-tag and a FLAG-tag inserted immediately after the alternative signal peptide derived from Interleukin-2 to facilitate protein expression. The HEK293F cells were cultured in SMM 293T-II medium (Sino Biological Inc.) at 37 °C under a 5% CO_2 atmosphere using a Zhichu shaking incubator (ZQWY-AS8E, 120 rpm). Upon reaching a cell density of 2.0×10^6 cells per ml, the pCAG-*ALKA* plasmids were transiently transfected into the cells. For a 1-liter HEK293F cell culture, approximately 2.0 mg of plasmids were pre-incubated with 4.0 mg of linear polyethylenimines (PEIs) (Polysciences) with a molecular weight of 25-kDa in 50 ml fresh medium for 20-30 minutes prior to transfection. The resulting mixture was then added to the cell culture and incubated for 48 hours before harvesting.

For purification, 16-litres HEK293F cells were harvested by centrifugation at 800g for 10 min and resuspended in the lysis buffer containing 25 mM HEPES (pH 7.4), 150 mM NaCl (lysis buffer A), 2.6 μg/ml aprotinin, 4 μg/ml pepstatin, and 2 μg/ml leupeptin. The lysate was incubated in the buffer containing 1%

Lauryl Maltose Neopentyl Glycol (LMNG, Anatrace) plus 0.1% cholesteryl hemisuccinate tris salt (CHS, Anatrace) at 4 °C for 2 hours for membrane protein extraction. After ultracentrifugation at 18,700g for 1 hour, the supernatant was collected and applied to the Anti-DYKDDDDK Tag (L5) Affinity Gel (BioLegend) at 4 °C for two time. The resin was washed six times with 5 ml wash buffer A (lysis buffer A plus 0.006% glycol-diosgenin (GDN, Anatrace)) each time. The protein was eluted with elution buffer A (wash buffer A plus 200 μg/ml FLAG peptide (GL Biochem). The eluent was incubated with nickel affinity resin (Ni-NTA, Qiagen) for 2 hours at 4 °C. The resin was washed with wash buffer B (lysis buffer A plus 0.006% GDN and 30 mM imidazole), and the protein was eluted with elution buffer B (lysis buffer A plus 0.006% GDN and 300 mM imidazole). The eluent was concentrated and a quarter was subjected to size-exclusion chromatography (SEC, Superose 6 Increase, 10/300, GE Healthcare) in a buffer containing 25 mM HEPES (pH 7.4), 150 mM NaCl, and 0.006% GDN. The peak fractions were pooled and concentrated to 14~16 mg/ml for the cryo-EM analysis. Similarly, the remaining three quarters were subjected to SEC in pH 10 buffer (25 mM CAPS, 150 mM NaCl, 0.006% GDN, pH 10.0), pH 11 buffer (25 mM CAPS, 150 mM NaCl, 0.006% GDN, pH 11.0), and pH 12.0 buffer (25 mM mixture of

Na_3PO_4 and Na_2HPO_4, 150 mM NaCl, pH 12.0), respectively. The peak fractions were then pooled and concentrated to 14-16 mg/ml for cryo-EM analysis.

Cryo-EM sample preparation and data acquisition

Aliquots (3.5 μL) of the protein sample were applied to glow-discharged holey carbon grids (Quantifoil Cu R1.2/1.3). The grids were blotted for 3.5 s and flash-frozen in liquid ethane cooled by liquid nitrogen using a Vitrobot (Mark IV, Thermo Fisher Scientific) at 8°C and 100% humidity. The prepared grids were transferred to a Titan Krios operating at 300 kV equipped with a Gatan K3 detector and a GIF Quantum energy filter. Movie stacks were automatically collected using EPU software (Thermo Fisher Scientific), with a slit width of 20 eV on the energy filter and a defocus range from -1.2 to -2.0 μm in super-resolution mode at a nominal magnification of 105,000×. Each stack was exposed for 2.56 s with an exposure time of 0.08 s per frame, resulting in a total of 32 frames per stack. The total dose rate was approximately 50 $e^-/Å^2$ for each stack. The stacks were motion-corrected with MotionCor2[27] and binned twofold, resulting in a pixel size of 0.827 Å/pixel. Meanwhile, dose weighting was performed[28]. The defocus values were estimated with Gctf[29].

Data processing

The contrast transfer function (CTF) estimation in cryoSPARC was performed using dose-weighted micrographs and Patch-CTF[30]. Template picker was employed for particle picking, utilizing templates derived from the 2D results generated by the initial particle picking with the blob picker tool. Accordingly, 1,039,627 particles were auto-picked from 2505 micrographs. Several rounds of 2D classification were performed and 357,224 good particles with different view directions were selected for Ab-initio reconstruction to generate initial references. Subsequently, Heterogeneous Refinement with C1 symmetry was performed using references generated from Ab-initio reconstruction. The yielded good particles were then were subjected to Non-uniform Refinement with C5 symmetry, finally generating a density map reported at an overall resolution of 2.86 Å using 175,938 particles. Resolutions were estimated using the gold-standard Fourier shell correlation (FSC) 0.143 criterion[31]. Local resolution variations were estimated in cryoSPARC.

Model building and structure refinement

The initial structure model for ALKA was generated using

AlphaFold[32], a state-of-the-art protein folding prediction algorithm. Subsequently, the predicted structure accurately positioned within the density map through molecular docking techniques. Manual adjustments and rebuilding of the ALKA structure were performed using COOT software[33]. Additionally, sequence assignment was primarily guided by bulky amino acid residues such as Phe, Tyr, Trp, and Arg to ensure accuracy. Furthermore, unique sequence patterns were exploited to validate the assigned residues. Structure refinements were carried out by Phenix in real space with secondary structure and geometry restraints[34]. The statistics of the 3D reconstruction and model refinement are summarized in Supplementary Table S1.

Acknowledgments

We thank the Cryo-EM Facility of Southern University of Science and Technology (SUSTech) for providing the facility support. This work was financially supported by the National Key R&D Program of China (2023YFD1700403 to H.S. and D.G.), the National Natural Science Foundation of China (32271254 to D.G.), and Tianjin Science and Technology Major Project (24ZXZSSS00170 to D.G.).

Author contributions

D.G. conceived and supervised the project. D.Q., H.S., R.Y., and D.G. designed the experiments. J.X., Y.J., M. G., Y. L., and W. L. performed the experiments. All authors contributed to the data analysis. D.G. wrote the manuscript.

Competing interests

The authors declare no competing financial interests.

Data and materials availability

The atomic coordinates and electron microscopy density maps of the three structures have been deposited in the PDB (http://www.rcsb.org) and the Electron Microscopy Data Bank (EMDB https://www.ebi.ac.uk/pdbe/emdb/). The accession numbers are as follows: PDB-21AB; EMD-67442. All other data are available from the corresponding authors upon reasonable request.

References

1 Jin, F. *et al.* Cryo-EM structure of the zinc-activated channel (ZAC) in the Cys-loop receptor superfamily. *Proc Natl Acad Sci U S A* **121**, e2405659121 (2024).
2 Lu, X. *et al.* Structural insights into the activation mechanism of the human zinc-activated channel. *Nat Commun* **16**, 442 (2025).
3 Thompson, A. J., Lester, H. A. & Lummis, S. C. The structural basis of function in Cys-loop receptors. *Q Rev Biophys* **43**, 449-499 (2010).
4 Chen, D. & Hawthorne, D. J. The cys-loop ligand-gated ion channel gene superfamily of the Colorado potato beetle,

Leptinotarsa decemlineata. *BMC Genomics* **26**, 702 (2025).

5 Buckingham, S. D., Biggin, P. C., Sattelle, B. M., Brown, L. A. & Sattelle, D. B. Insect GABA receptors: splicing, editing, and targeting by antiparasitics and insecticides. *Mol Pharmacol* **68**, 942-951 (2005).

6 Schnizler, K. *et al.* A novel chloride channel in Drosophila melanogaster is inhibited by protons. *J Biol Chem* **280**, 16254-16262 (2005).

7 Mounsey, K. E. *et al.* Molecular characterisation of a pH-gated chloride channel from Sarcoptes scabiei. *Invert Neurosci* **7**, 149-156 (2007).

8 Feingold, D., Starc, T., O'Donnell, M. J., Nilson, L. & Dent, J. A. The orphan pentameric ligand-gated ion channel pHCl-2 is gated by pH and regulates fluid secretion in Drosophila Malpighian tubules. *J Exp Biol* **219**, 2629-2638 (2016).

9 Redhai, S. *et al.* An intestinal zinc sensor regulates food intake and developmental growth. *Nature* **580**, 263-268 (2020).

10 Mi, T. *et al.* Alkaline taste sensation through the alkaliphile chloride channel in Drosophila. *Nat Metab* **5**, 466-480 (2023).

11 Kiwull-Schone, H., Kiwull, P., Manz, F. & Kalhoff, H. Food composition and acid-base balance: alimentary alkali depletion and acid load in herbivores. *J Nutr* **138**, 431S-434S (2008).

12 Park, S. J. & Ja, W. W. The basics of base sensing. *Nat Metab* **5**, 364-365 (2023).

13 Huang, A. L. *et al.* The cells and logic for mammalian sour taste detection. *Nature* **442**, 934-938 (2006).

14 Tu, Y. H. *et al.* An evolutionarily conserved gene family encodes proton-selective ion channels. *Science* **359**, 1047-1050 (2018).

15 Mi, T., Mack, J. O., Lee, C. M. & Zhang, Y. V. Molecular and cellular basis of acid taste sensation in Drosophila. *Nat Commun* **12**, 3730 (2021).

16 Hibbs, R. E. & Gouaux, E. Principles of activation and permeation in an anion-selective Cys-loop receptor. *Nature* **474**, 54-60 (2011).

17 Miller, P. S. & Aricescu, A. R. Crystal structure of a human GABAA receptor. *Nature* **512**, 270-275 (2014).

18 Chang, Y. C., Wu, W., Zhang, J. L. & Huang, Y. Allosteric activation mechanism of the cys-loop receptors. *Acta Pharmacol Sin* **30**, 663-672 (2009).

19 Bouzat, C. *et al.* Coupling of agonist binding to channel gating in an ACh-binding protein linked to an ion channel. *Nature* **430**, 896-900 (2004).

20 Yu, J. *et al.* Mechanism of gating and partial agonist action in the glycine receptor. *Cell* **184**, 957-968 e921 (2021).

21 Noviello, C. M. *et al.* Structure and gating mechanism of the alpha7 nicotinic acetylcholine receptor. *Cell* **184**, 2121-2134 e2113 (2021).

22 Mancinelli, R., Botti, A., Bruni, F., Ricci, M. A. & Soper, A. K. Hydration of sodium, potassium, and chloride ions in solution and the concept of structure maker/breaker. *J Phys Chem B* **111**, 13570-13577 (2007).

23 Kumar, A. *et al.* Mechanisms of activation and desensitization of full-length glycine receptor in lipid nanodiscs. *Nat Commun* **11**, 3752 (2020).

24 Wang, X., Li, G., Liu, J., Liu, J. & Xu, X. Z. TMC-1 Mediates Alkaline Sensation in C. elegans through Nociceptive Neurons. *Neuron* **91**, 146-154 (2016).

25 Murayama, T., Takayama, J., Fujiwara, M. & Maruyama, I. N. Environmental alkalinity sensing mediated by the transmembrane guanylyl cyclase GCY-14 in C. elegans. *Curr Biol* **23**, 1007-1012 (2013).

26 Pandey, P., Shrestha, B. & Lee, Y. Avoiding alkaline taste through ionotropic receptors. *iScience* **27**, 110087 (2024).

27 Zheng, S. Q. *et al.* MotionCor2: anisotropic correction of beam-induced motion for improved cryo-electron microscopy. *Nat Methods* **14**, 331-332 (2017).

28 Grant, T. & Grigorieff, N. Measuring the optimal exposure for single particle cryo-EM using a 2.6 A reconstruction of rotavirus VP6. *Elife* **4**, e06980 (2015).

29 Zhang, K. Gctf: Real-time CTF determination and correction. *J Struct Biol* **193**, 1-12 (2016).

30 Punjani, A., Rubinstein, J. L., Fleet, D. J. & Brubaker, M. A. cryoSPARC: algorithms for rapid unsupervised cryo-EM structure determination. *Nat Methods* **14**, 290-296 (2017).

31 Rosenthal, P. B. & Henderson, R. Optimal determination of particle orientation, absolute hand, and contrast loss in single-particle electron cryomicroscopy. *J Mol Biol* **333**, 721-745 (2003).

32 Jumper, J. *et al.* Highly accurate protein structure prediction with AlphaFold. *Nature* **596**, 583-589 (2021).

33 Emsley, P. & Cowtan, K. Coot: model-building tools for molecular graphics. *Acta Crystallogr D Biol Crystallogr* **60**, 2126-2132 (2004).

34 Adams, P. D. *et al.* PHENIX: a comprehensive Python-based system for macromolecular structure solution. *Acta Crystallogr D Biol Crystallogr* **66**, 213-221 (2010).

Figure legend

Fig. 1 | Overall structure of Drosophila ALKA chloride channel. a, Overall cryo-EM density map of the Drosophila ALKA channel determined under physiological pH conditions. ALKA assembles as a homopentamer. **b**, Overall structure of ALKA. The N-linked glycans are displayed as black sticks. All structural figures were prepared in PyMOL (www.pymol.org).

Fig. 2 | Structural features of ALKA. a, Topological diagram and overall structure showing one ALKA protomer. Four of the six loops forming the ligand-binding pocket in cysLGICs family are highlighted in the box. The ECD is composed of ten β-strands organized into an inner β-sheet and an outer β-sheet. **b**, Ligand binding is allosterically coupled to channel gating in cysLGIC family. The ligand-binding pocket, the ECD-TMD coupling interface, and the channel gating domain are indicated. **c**, K229 in loop C is a distinctive residue specific to the ALKA channel. The turn of ALKA loop C is inserted into the binding pocket and locked by interactions among K229 and E182 as well as Y124. d, Drosophila; h, Human; m, Mouse; c, *C. elegans*. **d**, Comparison of the conformation of loop C in ALKA with that of in zGlyRα1. Loop C of ALKA adopts an inward conformation, whereas the corresponding

loop in zGlyRα1 adopts an outward conformation. z, Zebrafish.

Fig. 3 | Structural architecture of the ion-conducting pore. a, The pore of ALKA under pH7.4 is closed. (Left) The ion permeation path, calculated by HOLE software, is illustrated as green dots. (Right) The pore radii of ALKA. **b**, A putative chloride ion is observed between the T280 and T284 rings, located closer to the T280 ring.

Fig. 4 | Structural mapping of lysine residues predicts the potential pH sensing residues. a, 11 out of the 12 lysine residues in the ECD of ALKA were reliably mapped to the structure. **b**, Summary of the locations and interacting residues for the 11 lysine residues. Four lysine residues (K149, K190, K192, and K229) are located around the ligand-binding pocket of the cysLGIC family, while K207 resides in the coupling region; all five are predicted to contribute to pH sensing and are highlighted in light blue. **c-f**, Ionic interactions mediated by the four lysine residues (K149, K190, K192, and K207) are indicated. **g**, Summarize the structural locations of the five lysine residues, highlighting that K229 is likely the principal pH sensor due to its strategic position in loop C.

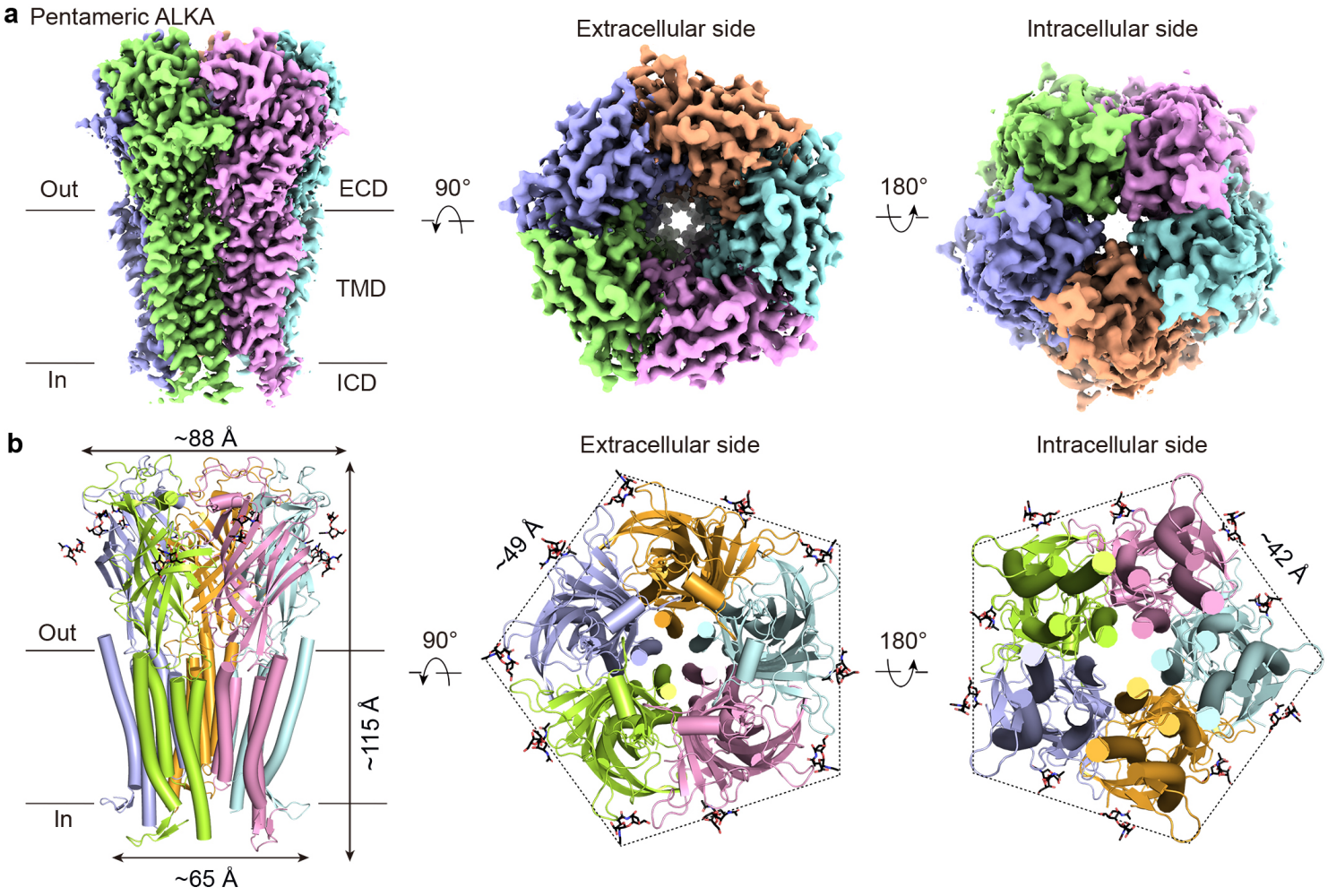
a Pentameric ALKA
Extracellular side
Intracellular side
Out
ECD
TMD
In
ICD
90°
180°
b
~88 Å
~115 Å
~65 Å
Out
In
Extracellular side
Intracellular side
~49 Å
~42 Å
90°
180°

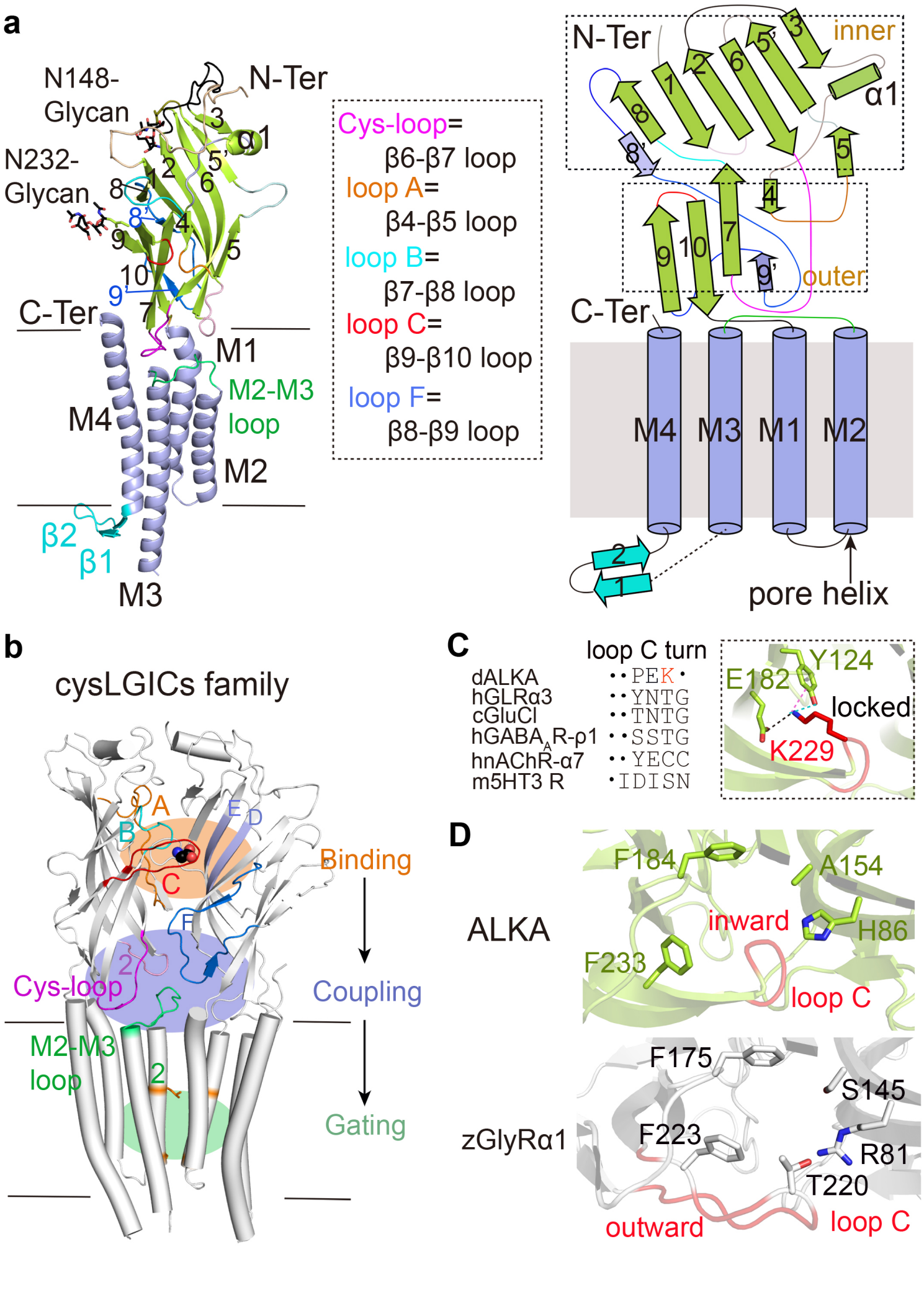
a
N148-Glycan
N232-Glycan
N-Ter
C-Ter
M1
M2-M3 loop
M4
M2
M3
β2
β1
Cys-loop= β6-β7 loop
loop A= β4-β5 loop
loop B= β7-β8 loop
loop C= β9-β10 loop
loop F= β8-β9 loop
inner
outer
pore helix
b
cysLGICs family
Binding
Coupling
Gating
Cys-loop
M2-M3 loop
C
loop C turn
dALKA ··PEK·
hGLRα3 ··YNTG
cGluCl ··TNTG
hGABA$_A$R-ρ1 ··SSTG
hnAChR-α7 ··YECC
m5HT3 R ·IDISN
Y124
E182
locked
K229
D
ALKA
F184
A154
inward
H86
F233
loop C
zGlyRα1
F175
S145
F223
R81
T220
outward
loop C

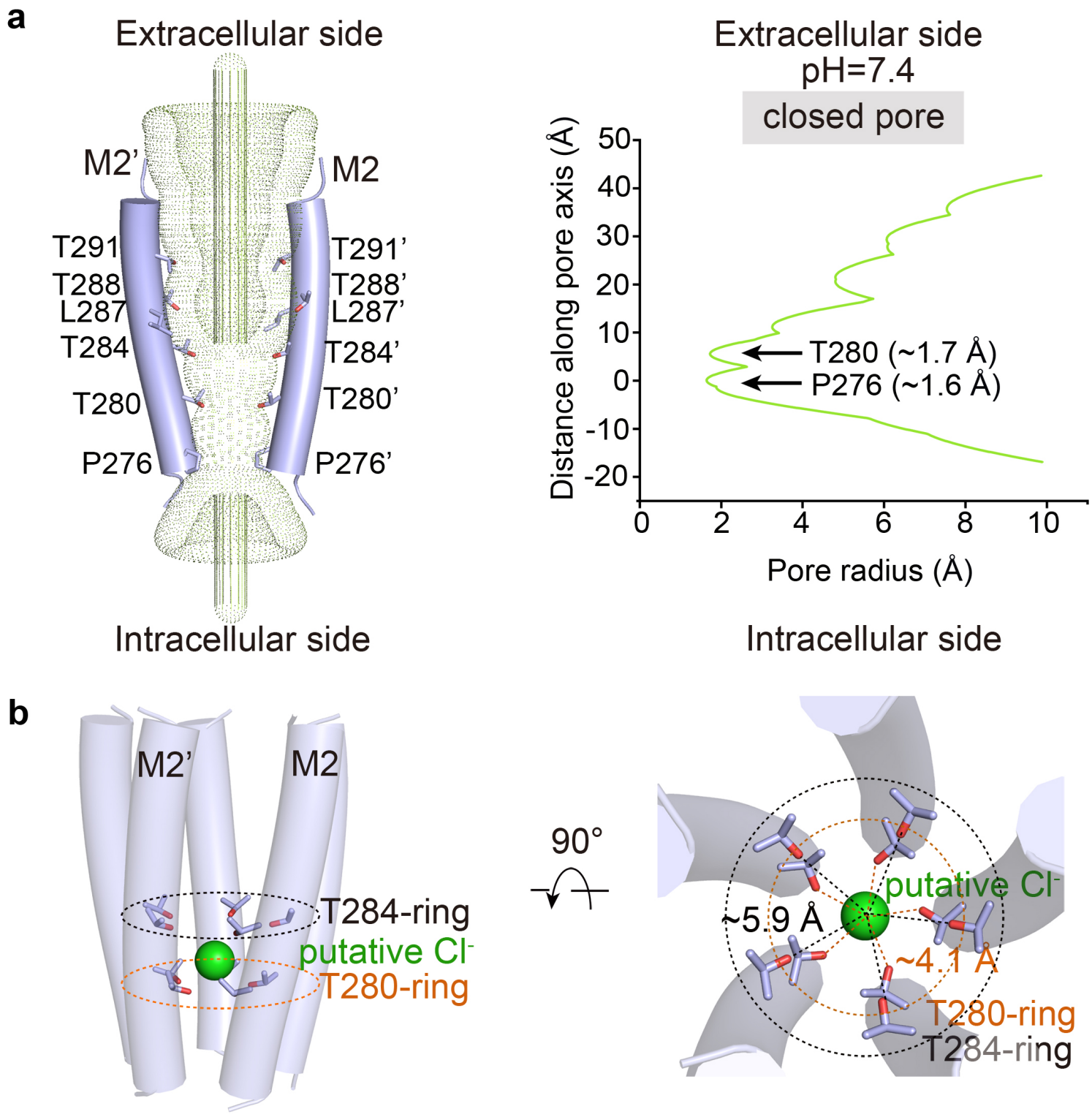
a
Extracellular side
M2'
M2
T291
T288
L287
T284
T280
P276
T291'
T288'
L287'
T284'
T280'
P276'
Intracellular side
Extracellular side
pH=7.4
closed pore
Distance along pore axis (Å)
50
40
30
20
10
0
-10
-20
0
2
4
6
8
10
Pore radius (Å)
T280 (~1.7 Å)
P276 (~1.6 Å)
Intracellular side
b
M2'
M2
T284-ring
putative Cl-
T280-ring
90°
putative Cl-
~5.9 Å
~4.1 Å
T280-ring
T284-ring

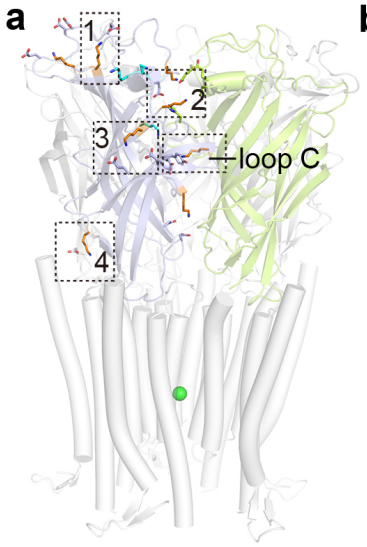

b

Locations	Lysine residues	Interacting residues
N-loop	K46	E113'_α1
	K53, K54	----
β5	K129	D76_loop1-2, D78_β2
loopβ5-β5'	K139	----
loopβ5'-β6	K147	D98, D99, E103_loop2-3
β6	K149	E95 _loop2-3
loop B	K190	E102', D105'_loop2-3
β8	K192	E221, D223_β9
loop F	K207	E166'_Cys-loop
loop C	K229	Y124_β4, E182_β7